Available online at www.sciencedirect.com
SCIENCE DIRECT
Journal of the European Ceramic Society 26 (2006) 1337–1349
www.elsevier.com/locate/jeurceramsoc

Reversible $\alpha' \leftrightarrow \beta'$ transformation in preferentially oriented sialon ceramics

Andrew Carman, Elena Pereloma, Yi-Bing Cheng *

School of Physics and Materials Engineering, Monash University, Vic. 3800, Australia

Received 7 October 2004; received in revised form 20 February 2005; accepted 25 February 2005
Available online 31 March 2005

Abstract

A preferential orientation was observed in a Nd-($\alpha + \beta$)-sialon ceramic, of the composition $Nd_{0.4}Si_{9.6}Al_{2.4}O_{1.2}N_{14.8}$, after hot pressing at 1800 °C for 2 h. Post-sintering heat treatment was performed at 1450 °C for 72 h, resulting in the $\alpha' \rightarrow \beta'$ transformation, accompanied by an increase in the M'_{ss} and 21R phases. Subsequent heat treatment at 1800 °C for 4 h resulted in a reverse transformation from β' to α', with a corresponding decrease in M'_{ss} and 21R. This indicates that the α' + liquid $\leftrightarrow \beta' + M'_{ss}$ + 21R transformation reaction is thermodynamically reversible. The microstructure was also found to be reversible, except for a certain degree of grain growth. The mechanical properties were determined from indentation tests, and were found to cycle with the transformation cycling. In addition, the preferred orientation introduced during hot pressing was observed in both the forward and reverse transformations, indicating that there is a crystallographic relationship between the transformation phases.

Keywords: Sialon; Hot pressing; Microstructure-final; Mechanical properties; Transformation cycling

1. Introduction

Sialon ceramics have been extensively studied because of their excellent properties, such as high strength and wear resistance, as well as for their ease of production. The addition of sintering aids, such as Al_2O_3 and rare-earth oxides, results in a liquid phase during sintering which produces a ceramic with good densification under pressureless conditions. This liquid, however, results in a residual grain boundary glass, which is detrimental to the high temperature properties of the material, such as the creep resistance. The amount of grain boundary glass may be greatly reduced by post-sintering heat treatment. Depending on the heat treatment temperature, the glass may be devitrified to form a more refractory secondary phase. This will then improve the high temperature properties of the material.

It was observed, however, that subjecting sialon ceramics to post-sintering heat treatments at 1000–1500 °C resulted in transformation of the α-sialon phase to the β-sialon phase.[1] It was also found that the reverse $\beta' \rightarrow \alpha'$ transformation could be promoted by heat treatment at 1775 °C. Therefore, there is the possibility of heat treating a mixed α/β-sialon ceramic in such a way as to achieve a desired microstructure, and therefore tailor the mechanical properties of the final material. The α' phase imparts hardness to the composite, due to the high hardness of α' resulting from the increased Burger's vector associated with the larger unit cell. The elongated β' grains increase the fracture toughness of the material by the mechanisms of crack deflection, crack bridging and grain pull-out.[2] The use of an α'/β' composite ceramic provides a number of advantages: the toughening of the material in situ through heat treatment avoids the need for extrinsic additives, such as whiskers and fibres, thereby, making fabrication easier, cheaper and safer. In addition, duplex α/β-sialons are easier to densify than pure α-sialon, again aiding production.[3]

There has been extensive research into the forward $\alpha' \rightarrow \beta'$ transformation, particularly in terms of the effect of stabilizing cation, composition, temperature and time.[1,4–6] The mechanical properties have also been studied in terms of

* Corresponding author.
E-mail address: Yibing.Cheng@spme.monash.edu.au (Y.-B. Cheng).

0955-2219/$ – see front matter © 2005 Elsevier Ltd. All rights reserved.
doi:10.1016/j.jeurceramsoc.2005.02.011

sialon phase assembly.[7,8] However, little work has been done on the reverse $\beta' \rightarrow \alpha'$ transformation, particularly its effect on the mechanical properties.[1,2] In addition, the crystallographic relationships between the transformation phases are not clear, nor is it known if such relationships exist. Polycrystalline sialon ceramics make investigating crystallographic relationships complex, due to the inherent randomness of the grain orientations. This may be overcome by introducing a preferred orientation into the ceramic during sintering. A preferred orientation has been introduced into a Ca-α-sialon,[10] however, the material was not heat treated to examine the effect of the $\alpha' \rightarrow \beta'$ transformation on the preferred orientation.

In this work, a preferred orientation was observed in a hot pressed Nd-sialon ceramic, which was then subjected to a number of cycles of the $\alpha' \leftrightarrow \beta'$ transformation. The effect of alternating forward and reverse transformation stages on the preferred orientation, microstructure and mechanical properties was investigated.

2. Experimental

The starting powders Si_3N_4 (H.C. Stark, Grade M11), AlN (H.C. Stark, Grade C), Al_2O_3 (Ajax Labchem) and Nd_2O_3 (Heraeus 99.9%) were measured out to give a composition of $Nd_{0.4}Si_{9.6}Al_{2.4}O_{1.2}N_{14.8}$, taking into account the surface oxides on the Si_3N_4 and AlN powders. The powders were milled using Si_3N_4 balls in isopropanol for 24 h and then dried. A hydraulic uniaxial press was used to make 1 in. pellets, which were then cold isostatically pressed at 200 MPa.

The samples were sintered by hot pressing at 1800 °C for 2 h under a load of 25 MPa, using a graphite die coated with BN for lubrication. The as-sintered ceramics were then subjected to alternating heat treatments at 1450 °C for 72 h and 1800 °C for 4 h to promote the forward $\alpha' \rightarrow \beta'$ and reverse $\beta' \rightarrow \alpha'$ phase transformations, respectively. Heat treatments at 1450 °C were performed in an alumina tube furnace under a high purity nitrogen atmosphere. Heat treatments at 1800 °C were carried out in a graphite resistance furnace, also under a high purity nitrogen atmosphere.

The surface layer (1.5–2 mm) was removed from the sample and the pellet was cut in half and a slice was cut off, as illustrated in Fig. 1, to allow analysis of the samples at orthogonal orientations. The samples were then polished to a mirror finish on a Struers RotoPol automatic polisher. Phase identification was carried out by X-ray diffraction (XRD) using a Phillips diffractometer with a Ni-filtered Cu Kα radiation source. X-ray diffraction was performed on both the top and side surfaces (as defined in Fig. 1) so as to obtain spectra perpendicular and parallel (respectively) to the hot pressing direction. A small amount of each sample was crushed and ground to a fine powder using a boron carbide mortar and pestle, before being mixed with a silicon reference powder. X-ray diffraction was then used to determine the lattice parameters of the α' and β' phases, using regression analysis. In addition, the random powder was used to determine the β' content, $\beta'/(\alpha' + \beta')$, as described by Gazzara and Messier.[11]

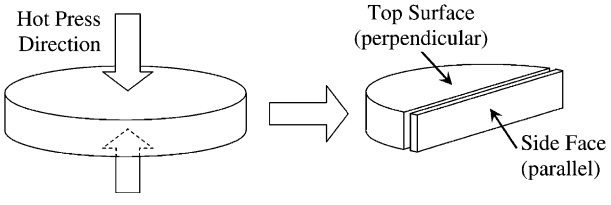

Fig. 1. Orientation of analysis plane, with respect to the hot pressing direction.

From the lattice parameters, the solid solution parameters (m and n for the α' phase and z for the β' phase) were calculated using the following equations:

For α-sialon of $Nd_{m/3}Si_{12-(m+n)}Al_{m+n}O_nN_{16-n}$:[12]

$$a\,(\text{Å}) = 7.752 + 0.036m + 0.02n \quad (1)$$

$$c\,(\text{Å}) = 5.620 + 0.031m + 0.04n \quad (2)$$

For β-sialon of $Si_{6-z}Al_zO_zN_{8-z}$:[13]

$$a\,(\text{Å}) = 7.603 + 0.0297z_a \quad (3)$$

$$c\,(\text{Å}) = 2.907 + 0.0255z_c \quad (4)$$

The average value of z_a and z_c was determined and used as the solid solubility in the present work.

After application of a carbon coating, microstructural analysis was performed on a Philips XL30 SEM using backscattered electron imaging. Distribution of the AlN polytypoid phase was determined by X-ray mapping on a JEOL JSM 840A fitted with an Oxford EDXS detector. Image analysis of SEM micrographs was then used to determine the volume fractions of the secondary phases present in the samples.

The density was determined using Archimedes' principle in water. A sintered pellet was cut into four wedges. All of the wedges were subjected to all heat treatments at the same time. The surfaces were removed from all four wedges after each heat treatment stage so as to remove any surface effects, and the density of each wedge was measured to give an average value.

The Vickers hardness and fracture toughness of the samples were measured by indentation using a Vickers diamond indenter under a load of 10 kg. The hardness and toughness were determined using the method of Anstis et al.[14]

3. Results and discussion

The samples were identified according to the stage at which they were removed during the transformation cycling: AS for as-sintered, F1 for forward $\alpha' \rightarrow \beta'$ transformation 1, R1 for reverse $\beta' \rightarrow \alpha'$ transformation 1, and so on. Table 1 indicates the heat treatment schedules used for the samples in this study.

Table 1
Heat treatment programs and resultant sample identification

	Hot press		α′ → β′ [1]		β′ → α′ [1]		α′ → β′ [2]		β′ → α′ [2]		α′ → β′ [3]		β′ → α′ [3]
AS	1800 °C/2h												
F1	1800 °C/2h	→	1450 °C/3d										
R1	1800 °C/2h	→	1450 °C/3d	→	1800 °C/4h								
F2	1800 °C/2h	→	1450 °C/3d	→	1800 °C/4h	→	1450 °C/3d						
R2	1800 °C/2h	→	1450 °C/3d	→	1800 °C/4h	→	1450 °C/3d	→	1800 °C/4h				
F3	1800 °C/2h	→	1450 °C/3d	→	1800 °C/4h	→	1450 °C/3d	→	1800 °C/4h	→	1450 °C/3d		
R3	1800 °C/2h	→	1450 °C/3d	→	1800 °C/4h	→	1450 °C/3d	→	1800 °C/4h	→	1450 °C/3d	→	1800 °C/4h

3.1. As-sintered material

The XRD spectra for the planes perpendicular and parallel to the hot pressing direction in the as-sintered material are shown in Fig. 2. The phases present in the as-sintered sample are α′, β′, 21R and M'_{ss}, with α′ clearly the majority phase, as observed previously in a similar composition.[15] The presence of a preferred orientation in the hot pressed ceramic can be seen by comparing the spectra in the two orthogonal planes. The (2 1 0) and (1 0 2) reflections for the α′ phase clearly show different relative intensities perpendicular and parallel to the hot pressing direction. The (2 1 0) reflection, which is parallel to the *c*-axis of the unit cell, is stronger normal to the hot pressing direction, whereas the (1 0 2) reflection, which intersects the *c*-axis, is stronger parallel to the pressing direction. This indicates that the *c*-axis preferentially lies in the plane perpendicular to the hot pressing direction. A similar preferential orientation can also be seen for the β′ phase by comparing the relative intensities of the (2 1 0) and (1 0 1) reflections. As the *c*-axis is the growth direction for both the α′[16] and β′[17] phases, it appears that the external pressure applied during sintering has hindered the grain growth and forced the grains to preferentially grow perpendicular to the hot pressing direction.

Scanning electron microscopy was performed on the surfaces perpendicular and parallel to the hot pressing direction, as seen in Fig. 3. The white phase is the Nd-rich grain boundary glass, the grey phase is α′, and the dark grains are either β′ or 21R (as neither phase contains the rare-earth element). The SEM micrograph of the top surface shows a uniform, homogenous microstructure, while the microstructure of the side face illustrates the preferred orientation normal to the hot pressing direction (indicated by the arrow) as evidenced by the prevalence of grains oriented along or close to the horizontal direction. The micrographs indicate the elongated morphology of the α′ phase that develops as a result of the pressure applied during sintering. Both micrographs show a fine, uniform distribution of grain boundary glass, and confirm that α′ is the majority phase in the sample.

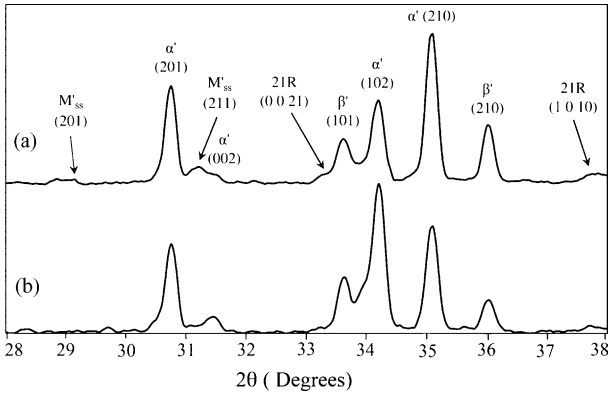

Fig. 2. Spectra of AS sample (a) perpendicular and (b) parallel to the hot pressing direction.

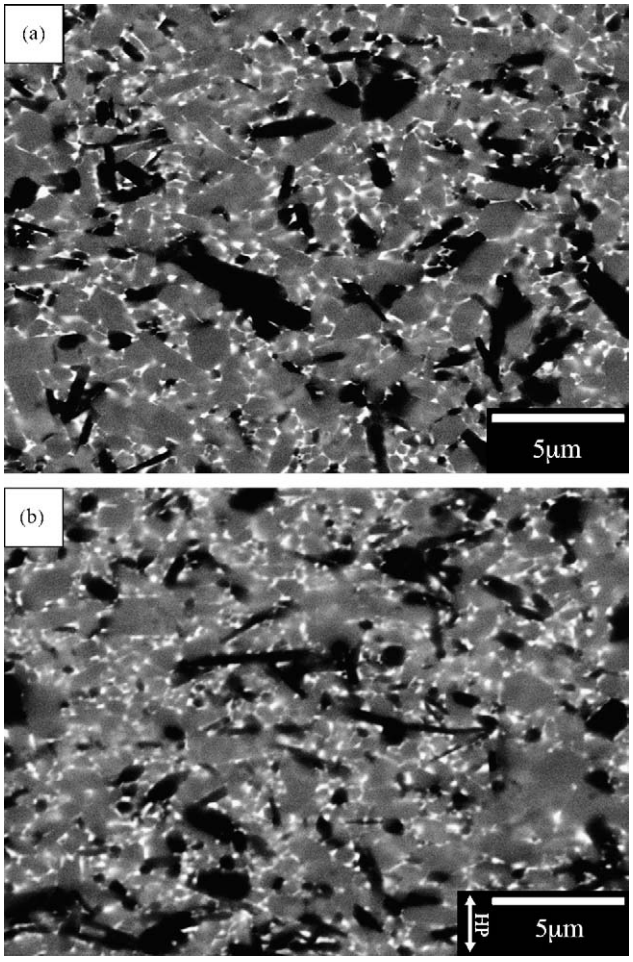

Fig. 3. SEM images of AS sample (a) perpendicular and (b) parallel to the hot pressing direction.

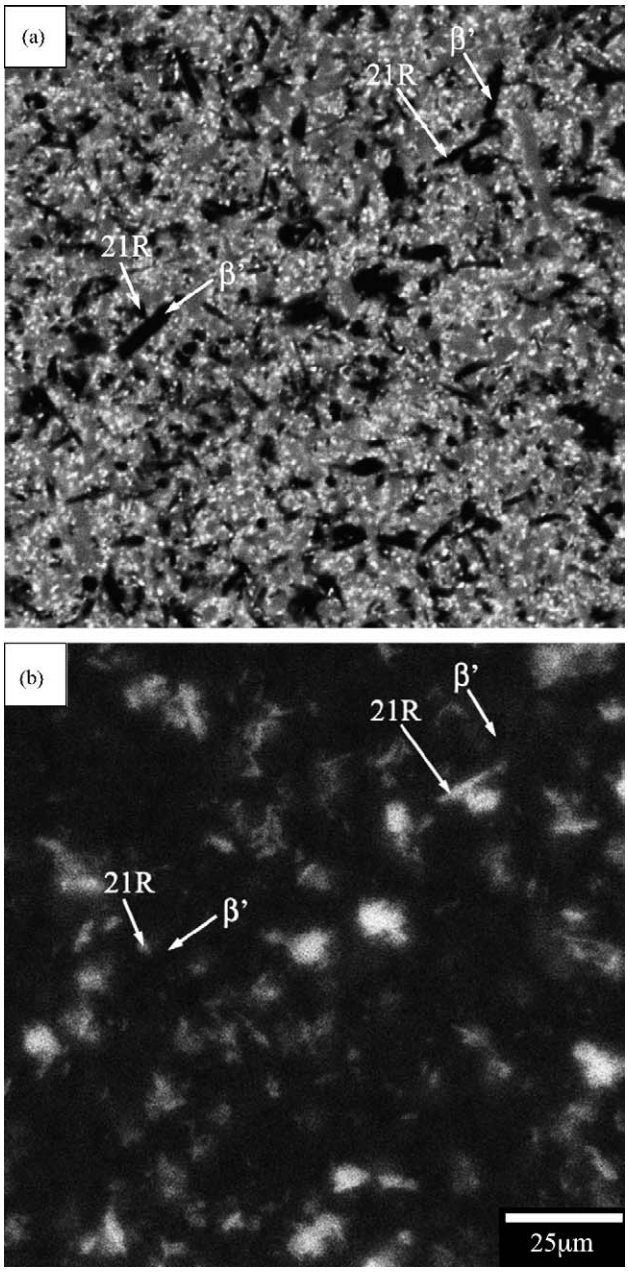

Fig. 4. (a) Back-scattered electron image and (b) accompanying Al X-ray map for AS sample.

Both the β′ and 21R phases appear dark in back-scattered electron imaging as neither phase contains neodymium. Identification by their morphology is also unreliable, particularly when subsequent heat treatment leads to transformation and grains coalesce and impinge on one another. It has been shown that, as 21R has a much higher aluminum content, elemental X-ray mapping of aluminium can be used to differentiate β′ and 21R.[18] Fig. 4 shows the back-scattered electron image with the corresponding aluminium X-ray map of the as-sintered material. The β′ and 21R are clearly distinguishable by comparing the two images and noting the contrast in the Al X-ray map. Using this method of distinguishing β′ and 21R, image analysis may be used to determine the volume fractions of all the phases present, which are shown in Table 2.

Table 2
Volume fractions of phases present in AS, F1 and R1 samples

	α′	β′	21R	Nd-rich[a]
AS	76	11	8	4.6
F1	20	53	16	9
R1	67	15	13	4.7

[a] Nd-rich refers to grain boundary glass in AS and R1 samples, or M'_{ss} in F1 sample.

3.2. Forward α′ → β′ transformation

Heat treatment of the as-sintered sample at 1450 °C resulted in the α′ → β′ transformation, as evidenced by the significant increase in β′. This increase in β′ can be seen in both the XRD spectra in Fig. 5(a) and the SEM micrograph in Fig. 5(b). Comparison of the XRD spectra in Fig. 5(a) to that in Fig. 2 indicates that β′ becomes the majority phase after heat treatment at 1450 °C for 72 h, with only a small amount of α′, and that an increase in M'_{ss} has accompanied the α′ → β′ transformation. More interestingly, the preferred orientation

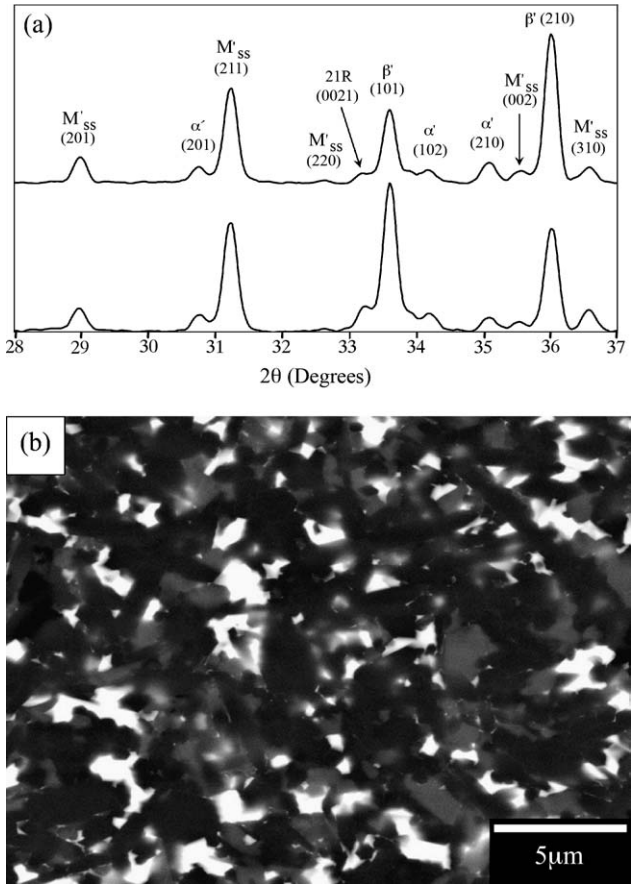

Fig. 5. Results for F1 sample (a) XRD spectra perpendicular and parallel to the hot pressing direction and (b) SEM image of the top surface.

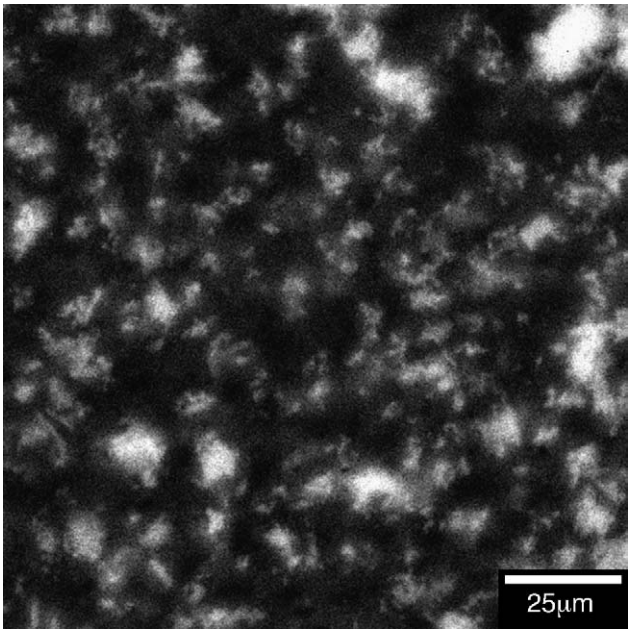

Fig. 6. Aluminium X-ray map of F1 sample.

is still observed in the β′ phase after α′ → β′ transformation, as seen by the stronger β′ (2 1 0) reflection perpendicular to the hot pressing direction as compared to that in the surface parallel to the pressing direction. The preferred orientation has been maintained during the α′ → β′ transformation under pressureless heat treatment conditions, suggesting a crystallographic relationship between the transformation phases. A large number of β′ grains with an elongated morphology have been observed in the transformed sample. This morphological characteristic for the β′ grains was mainly inherited from the elongated α′ grains in the as-sintered sample. However, comparison of Figs. 3(a) and 5(b) seems to indicate that the β′ grains in the transformed sample have a greater aspect ratio than the α′ grains in the as-sintered sample. This suggests that there has been a degree of grain growth along the *c*-axis, which is unexpected at the heat treatment temperature of 1450 °C.

In addition to the increased β′ content, the SEM micrograph in Fig. 5(b) also indicates that the fine, uniformly dispersed grain boundary glass seen in Fig. 3 has been replaced by larger pockets of agglomerated M'_{ss} (white). This suggests that the grain boundary glass migrates during heat treatment and agglomerates to form the secondary phase. This grain boundary migration is most likely due to dewetting of the grain boundary at the heat treatment temperature, accompanied by reductions in the free energy associated with devitrification of the glass and minimising the surface area to volume ratio.

The Al X-ray map of the F1 sample is shown in Fig. 6 and it is clear that there has been an increase in 21R when compared to that in Fig. 4(b). Image analysis was again used to determine the volume fractions of the phases present. From Table 2, it is seen that the 4.6 vol.% grain boundary glass found in sample AS has increased to 9.0 vol.% M'_{ss} after heat treatment at 1450 °C. This indicates that the amount of M'_{ss} formed during heat treatment cannot solely be due to devitrification of the grain boundary glass, but also a result of the α′ → β′ transformation. The Nd and Al expelled from the α′ phase during the phase transformation are, therefore, incorporated into the M'_{ss} and 21R, respectively. Hence, the full transformation path previously proposed in the Sm-sialon system[19] is confirmed to be the decomposition of the metastable α-sialon phase through reaction with the grain boundary liquid, as given by:

$$\alpha' + liquid \rightarrow \beta' + M'_{ss} + 21R \quad (5)$$

This reaction involves the dissolution of α′ into the liquid phase (glass) and precipitation of β′ and 21R. It is likely that the significant compositional change in the residual liquid after the solution–precipitation process makes the liquid phase unstable and crystallization occurs at, or immediately below, the heat treatment temperature. The α′ phase was initially formed in the system at 1800 °C. Its re-dissolution into the grain boundary liquid at a temperature much lower than the initial sintering temperature suggests that the α′ composition is metastable and will decompose when a liquid phase appears to allow significant diffusion. In the present system this occurs below approximately 1600 °C.[20]

3.3. Reverse β′ → α′ transformation

Subsequent heat treatment of the F1 sample at 1800 °C resulted in a marked decrease in the β′ content of the material, as shown in Fig. 7. The XRD spectra in Fig. 7(a) clearly show a reduction in β′ and a corresponding increase in the α′ phase. This confirms the reversibility of the α′ ↔ β′ transformation already reported.[1,9] In addition, the M'_{ss} peaks in the XRD spectra have decreased, suggesting a melting of the M'_{ss} at the elevated heat treatment temperature. The reduction in the amount of grain boundary phase can be confirmed by comparing SEM images in Figs. 5(b) and 7(b). The R1 microstructure is similar to that of AS (in Fig. 3(a)), except for having slightly coarser grain boundary glass junctions and a certain degree of sialon grain growth. The agglomerated M'_{ss} observed in F1 has been melted and has re-wet the grain boundaries, thereby, producing a fine, uniformly distributed grain boundary glass on cooling. It can also be seen that α′ is, indeed, the majority phase. Agglomeration of the M'_{ss} and subsequent melting and re-wetting of the grain boundary glass has been previously observed in the Nd-system,[9] however, no reverse transformation was observed at the lower heat treatment temperature of 1750 °C with the shorter heat treatment time of 1 h. Reverse transformation has been demonstrated in a Nd-α/β-sialon, however, evidence of melting the melilite and re-wetting the α- and β-sialon grains was not clear.[2]

Comparison of the XRD spectra in Fig. 7(a) indicates that the preferred orientation observed in previous samples is still maintained, even though all post-sintering heat treat-

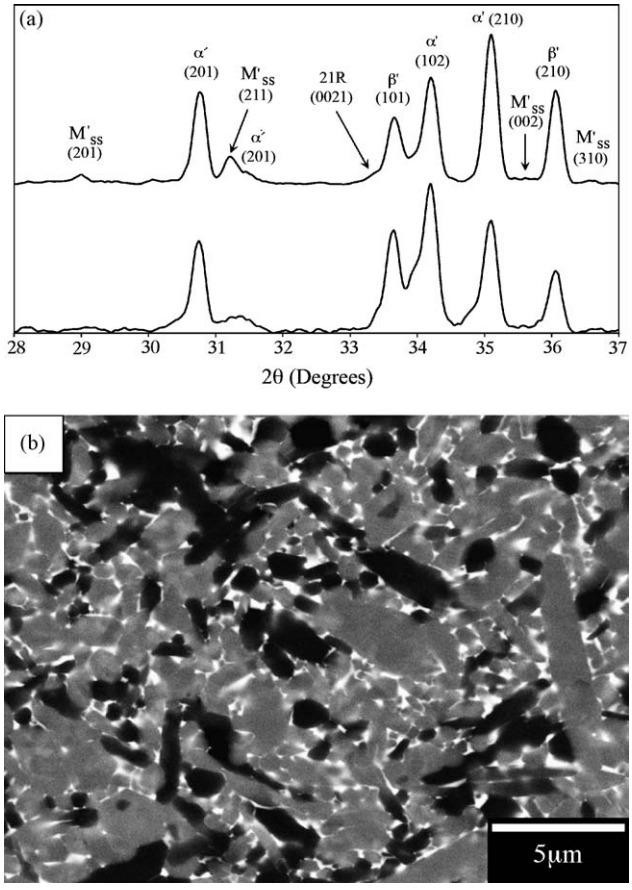

Fig. 7. Results for R1 sample (a) XRD spectra perpendicular and parallel to the hot pressing direction and (b) SEM image of the top surface.

ments have been performed under pressureless conditions. This suggests that a crystallographic relationship between the transformation phases exists in both the forward and reverse transformation routes. Both α′ and β′ phases have a hexagonal symmetry with very similar *a* dimensions in the lattices and only differ significantly in the *c* dimension. Therefore, it is thought that the α′ ↔ β′ phase transformation may nucleate on a crystal plane common to both, followed by growth along a certain crystallographic direction. There has been TEM evidence for epitaxial nucleation of α-sialon on α-Si_3N_4 grains,[21] and β-sialon on α-Si_3N_4, β-Si_3N_4 or other β-sialon grains[17] during sintering. Detailed TEM work is required to ascertain if similar relationships exist between α- and β-sialon during the reversible α′ ↔ β′ phase transformation.

Fig. 8 shows the Al X-ray map of R1, indicating that the 21R content has decreased during the reverse β′ → α′ transformation. Image analysis confirms this (Table 2). The simultaneous decrease in β′, M'_{ss} and 21R confirms not only the reversibility of the α′ ↔ β′ as reported previously,[1,2] but the reversibility of the reaction path given in Eq. (5) to give:

$$\alpha' + liquid \leftrightarrow \beta' + M'_{ss} + 21R \quad (6)$$

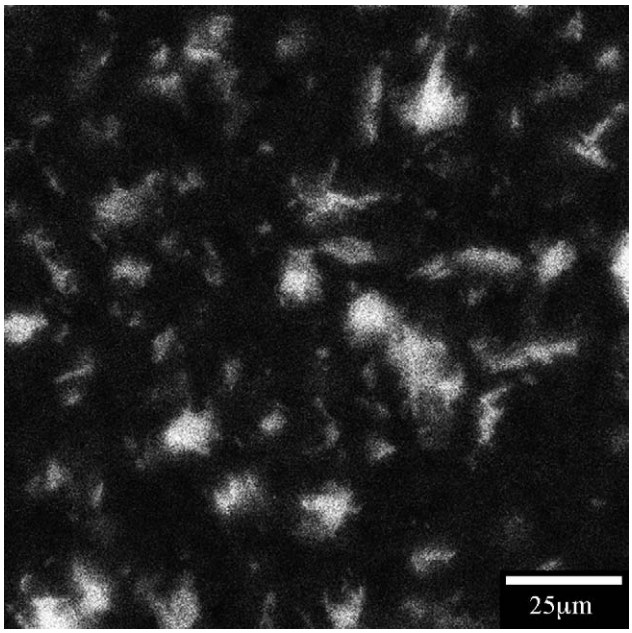

Fig. 8. Aluminium X-ray map of sample R1.

During the reverse transformation Nd must diffuse into the α′ to stabilise the phase. The primary source of Nd is the M'_{ss} phase, which will decrease in amount as Nd is removed. This is supported by image analysis which indicates that the volume fraction of grain boundary glass in R1 is 4.7 vol.%, much lower than that in F1 and very close to that of the as-sintered sample. Because the reverse transformation requires the melting of M'_{ss} this process can only occur above 1750 °C for the Nd sialon system.[22] At this temperature the kinetics of the phase transformation is high, which is aided by the low viscosity of the liquid, providing enhanced diffusion.

3.4. Transformation cycling

Two more cycles of the α′ ↔ β′ transformation were performed by alternating the 1450 °C and 1800 °C heat treatments. The phase contents during transformation cycling are summarised in Fig. 9 which indicates that the reversibility of

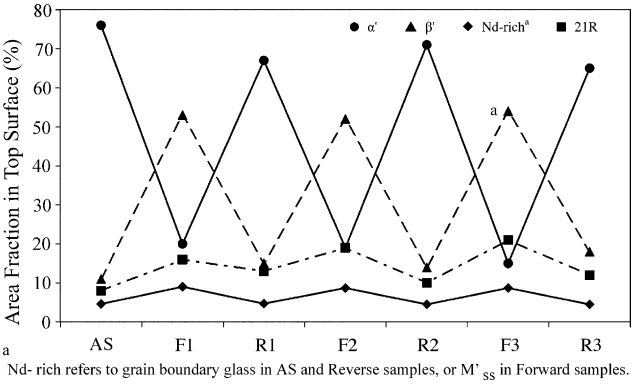

Fig. 9. Volume fractions of phases present in Nd-sialon during transformation cycling.

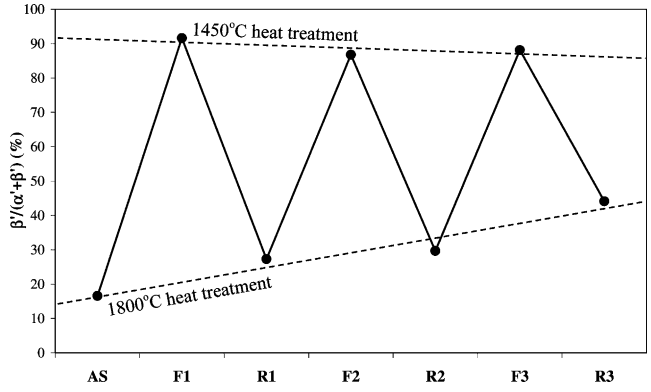

Fig. 10. Volume fraction of sialon phase in β′ form during transformation cycling.

Eq. (6) persists for a number of cycles. During all heat treatments at 1450 °C, the α′ decreases while the β′ increases, accompanied by an increase in M'_{ss} and 21R, as governed by the forward transformation route in Eq. (5). All heat treatments at 1800 °C result in an increase in the α′ content while the β′, M'_{ss} and 21R phases decrease, following the reverse transformation route.

If the β′/(α′ + β′) volume fraction is plotted for the samples during transformation cycling, a more interesting trend is observed, as shown in Fig. 10. Again, the forward transformation heat treatments at 1450 °C resulted in a marked increase in β′ content while the reverse transformation at 1800 °C for 4 h led to a reduction in the β′ volume fraction. However, the minimum β′ contents after reverse transformation appear to increase as the cycles progress, while the maximum β′ contents after forward transformation decrease, although to a much lesser extent. This suggests that the α′ ↔ β′ transformation becomes more sluggish after successive transformation cycles.

The reduced kinetics of the transformation may be the result of grain growth. The forward α′ → β′ transformation requires the stabilising cation (Nd) to diffuse out of the α′ grains and into the grain boundary glass, which then devitrifies to form M'_{ss}. The reverse β′ → α′ transformation requires the M'_{ss} to melt, thereby, supplying "free" Nd to diffuse in to the α′ grains to stabilise the phase. Grain growth will, effectively, increase the diffusion path between the sialon grains and the grain boundary phase, thereby, decreasing the rate at which Nd may diffuse into or out of the grain. In addition, the grain growth leads to larger pockets of glass or M'_{ss} that are farther apart, thereby, further hindering diffusion between the sialon grains and the grain boundary phase and decreasing the kinetics of transformation.

SEM imaging confirms the microstructural reversibility of the α′ ↔ β′ transformation, though to a limited degree. The forward transformation at 1450 °C results in agglomerated M'_{ss} forming with β′ being the majority phase. Reverse transformation at 1800 °C melts the M'_{ss} and produces a microstructure with a fine, uniformly distributed grain boundary glass and a majority of α′ phase. However, successive cycles

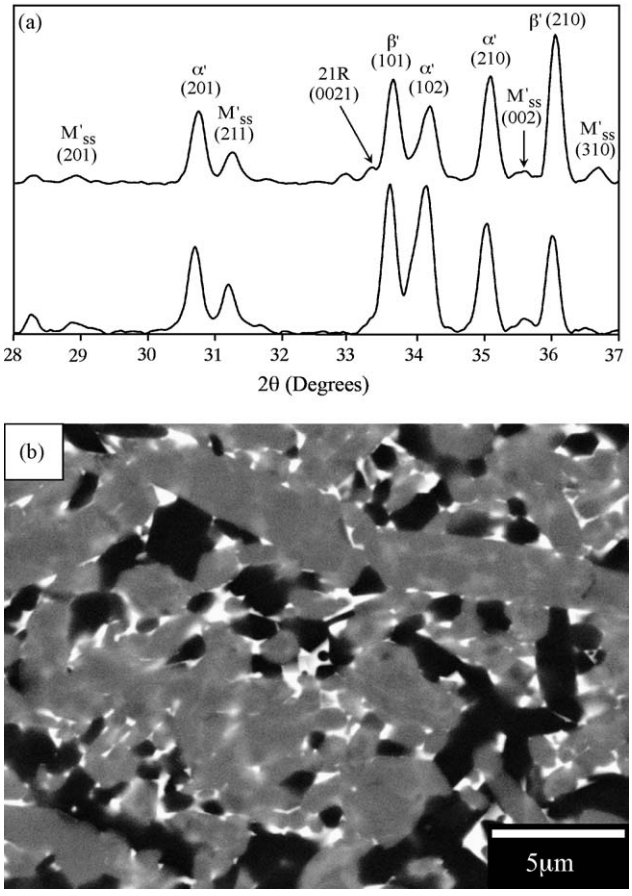

Fig. 11. Results for R3 sample (a) XRD spectra perpendicular and parallel to the hot pressing direction and (b) SEM image of the top surface.

result in grain growth, which leads to a coarser microstructure, including the grain boundary glass junctions, as shown in Fig. 11(b). The glass pockets become coarser because of the grain growth associated with heat treatment at 1800 °C, which limits the packing efficiency of the grains.

Fig. 11(a) shows the XRD spectra of the top surface and the side face of the sample that has undergone three cycles of the phase transformation. Again, the (2 1 0) reflection is stronger in the plane perpendicular to the original hot pressing direction, indicating that the preferred orientation is still present after three cycles of the α′ ↔ β′ transformation. This indicates that the crystallographic relationship between the transformation phases is maintained during all stages of the transformation cycling.

Lattice parameter measurements for the α′ and β′ phases are shown in Fig. 12. All of the graphs have a *y*-axis of 0.02 Å to make comparison between graphs easier. Therefore, it is immediately obvious that the α′ phase shows a greater spread of lattice parameter values than β′. More interestingly, the *a*-axis and, to a lesser extent, the *c*-axis lattice parameters of α′ fluctuate regularly with successive stages of the transformation cycling. Lines of best fit have been included, showing a strong trend for increasing *a* and *c* parameters in α′, while the *a*-axis of β′ shows a weaker increase and the *c*-axis is

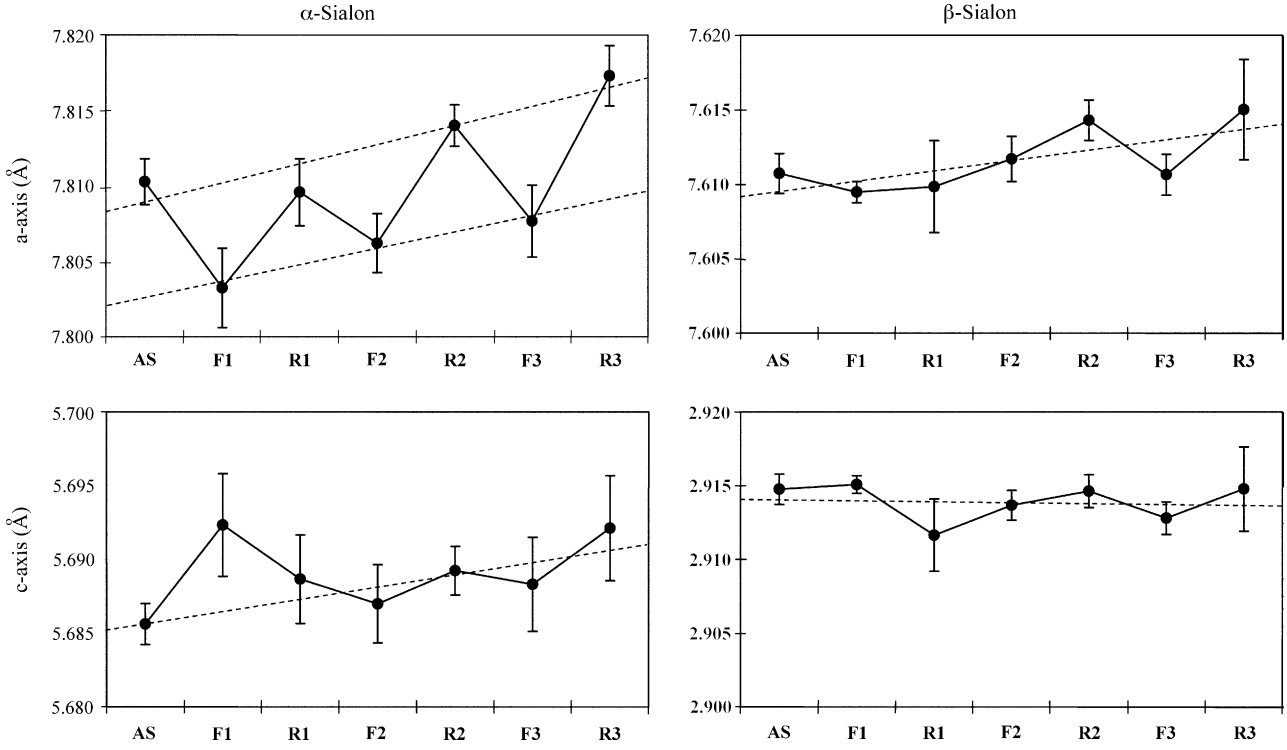

Fig. 12. Lattice parameters for the *a*- and *c*-axes of the α′ and β′ phases during transformation cycling.

almost constant. It should be noted that the line of best fit for the *c*-axis of α′ was determined ignoring the anomalous value for the F1 sample.

The trend for increasing *a* and *c* parameters in α′ and β′ suggests non-equilibrium conditions. It is clear that the forward transformation does not reach equilibrium as not all α′ is transformed to β′, which is expected at 1450 °C. However, reverse transformation also does not seem to reach equilibrium, even after 4 h of heat treatment at 1800 °C, because the as-sintered α′:β′ ratio is never reached. In fact, additional work by the authors has shown that even after 8 h of heat treatment at 1800 °C, the as-sintered α′:β′ ratio is not reached. The kinetics of transformation are very high at 1800 °C, however, the driving force for reverse transformation appears to be low. This is due to the poor stability of Nd-α-sialon, in conjunction with the effects of secondary phases such as M'_{ss}. The free energy of the sialon phases is shown schematically in Fig. 13, where the driving force for transformation is given by the free energy change ΔG. At 1450 °C, β′ is more thermodynamically stable and $\Delta G_{\alpha' \rightarrow \beta'}$ is large, so that α′ → β′ transformation readily occurs. At 1800 °C, α′ becomes the more stable phase, however, $\Delta G_{\beta' \rightarrow \alpha'}$ is small as the thermodynamic temperature for reverse transformation (T_R) is close to the heat treatment temperature. In addition, the need to melt M'_{ss} to provide the stabilising cation for transformed α′ provides another barrier to transformation.

The general trend to increasing lattice parameters for consecutive forward or reverse transformations can, therefore, be explained in terms of kinetics. Forward transformation occurs at 1450 °C, where the diffusion rate will be limited for sialon ceramics, whereas the reverse transformation is observed at 1800 °C, where diffusion rates are dramatically increased. Therefore, the compositional change will occur more rapidly during the reverse transformation and a greater extent will be observed than during the forward transformation. Thus, a net increase in the lattice parameters results from the greater substitution. The successive increase in the lattice parameters of α′ is inversely proportional to the amount of α′ in the sample with the consecutive transformation cycling, but the amount of M'_{ss} remains almost unchanged. This suggests that the amount of Nd in the α′ phase has increased because there

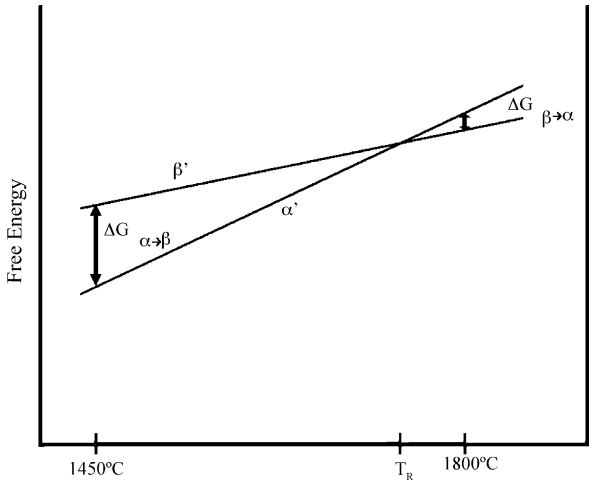

Fig. 13. Schematic free energy diagram of sialon phases, where T_R is thermodynamic reverse transformation temperature.

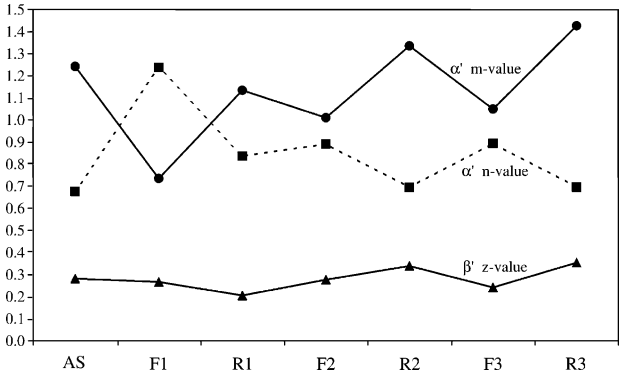

Fig. 14. Solid solution parameters of α- and β-sialon phases during transformation cycling.

is more Nd available for relatively less amounts of α′ to be stabilised.

The *m*- and *n*-values of the α′ phase and the *z*-value of the β′ phase are shown in Fig. 14 for the Nd-sialon during transformation cycling. It is clear that the composition of α-sialon varies with heat treatment in much the same way as the lattice parameters. Forward transformation at 1450 °C leads to a decrease in the *m*-value while the *n*-value increases. Reverse transformation at 1800 °C results in the *m*-value increasing and the *n*-value decreasing. The contraction of the α′ phase field at lower temperatures suggests that the *m*-value should increase and the *n*-value would decrease after heat treatment at 1450 °C, contrary to the behaviour observed. However, it should be noted that the remaining α′ phase at 1450 °C is metastable and will fully transform to β′ if given time to reach equilibrium. Therefore, it may be expected that the α′ phase composition will adjust so as to approach that of the β′ phase. Conversely, heat treatment at 1800 °C will result in reverse transformation as the α′ phase field expands and the sample composition lies in the α′-β′-21R-M'_{ss} compatibility tetrahedron.

This can be seen in Fig. 15, where the *m*- and *n*-values are plotted on the α′-plane. Heat treatment at 1450 °C to induce the α′ → β′ transformation results in the composition moving towards the β′ phase line on the *n*-axis, while the reverse transformation at 1800 °C leads to the composition moving away from the β′ line and towards the α′ phase field. β-Sialon, on the other hand, shows much less variation in composition as a result of alternating heat treatments, indicating

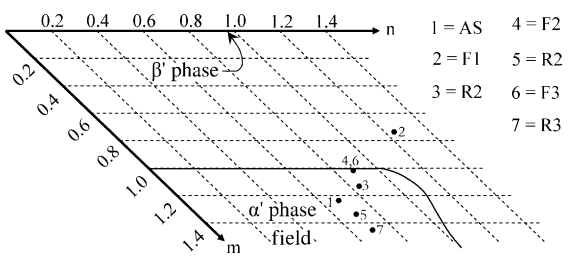

Fig. 15. *m*- and *n*-values of α′ phase during transformation cycling, plotted on the α′ plane.

that β′ has a more stable composition during transformation cycling.

3.5. Mechanical properties

The hardness and fracture toughness of the hot pressed and heat-treated samples are given in Fig. 16 for the top surface. There is clearly a cyclical pattern to the mechanical properties as a function of transformation cycling stage, which resembles the α′ ↔ β′ phase change cycling in Fig. 9. Thus, the change of α′ and β′ contents resulting from the forward and reverse phase transformations clearly affects the mechanical properties in a reliable fashion. As the forward α′ → β′ transformation proceeds during heat treatment at 1450 °C, the α′ content decreases, thereby, decreasing the hardness of the ceramic. Since both the α′ and β′ grains have elongated morphologies, it would be expected that the toughness would not change significantly, possibly decreasing as a result of the agglomeration of the grain boundary phase. In fact, the α′ → β′ transformation is accompanied by an increase in toughness, supporting the observation that the transformed β′ has a greater aspect ratio than the parent α′ phase. The greater aspect ratio enhances the toughening mechanisms of the phase, thereby, increasing the fracture toughness of the material.

It can also be seen in Fig. 16(a) that the hardness shows a general trend to decrease for successive heat treatments. This is primarily a result of grain growth during the 1800 °C heat

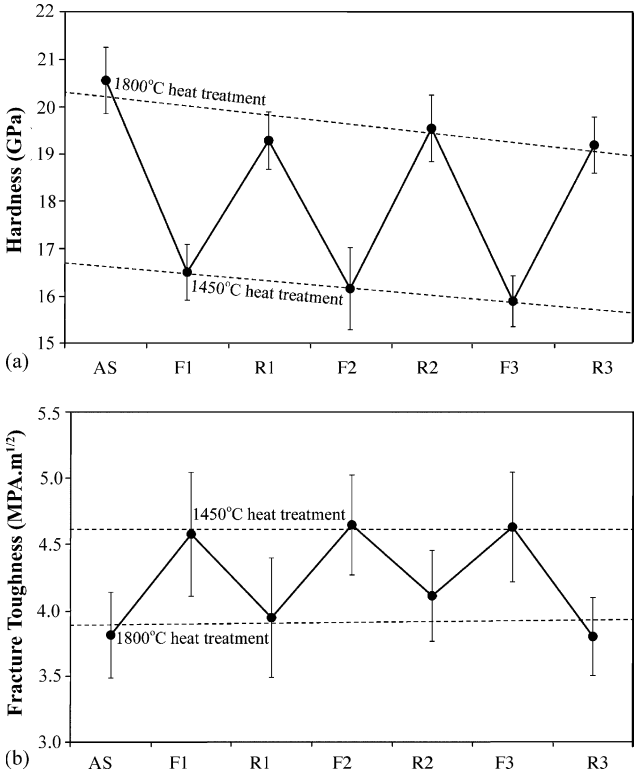

Fig. 16. (a) Vickers hardness and (b) fracture toughness of top surfaces of samples during transformation cycling.

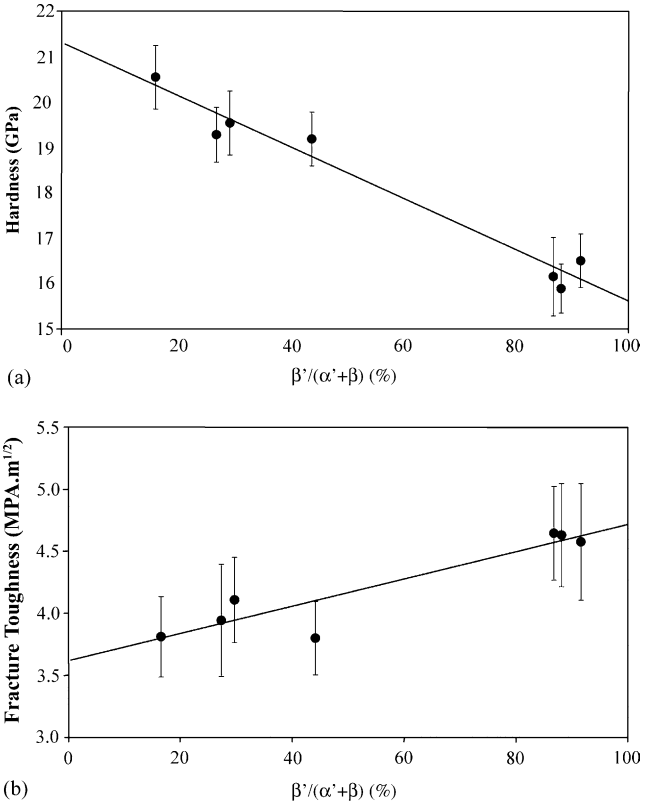

Fig. 17. (a) Vickers hardness and (b) fracture toughness of the Nd-sialon as a function of β′ volume fraction.

treatments, which will tend to decrease the hardness of the material. Interestingly, the toughness remains relatively constant after successive heat treatments at 1450 °C or 1800 °C. Grain growth will tend to increase toughness in microstructures with elongated morphologies. However, the aspect ratio of the β′ grains may decrease on successive cycles of the $\alpha' \rightarrow \beta'$ transformation and decrease the toughness, thereby, counteracting the effect of grain growth.

The relationship between the α′ and β′ volume fractions and the mechanical properties is evident in Fig. 17, which plots the volume fractions in Fig. 10 against the hardness and fracture toughness results in Fig. 16. There is a definite linear relationship to the α′ and β′ contents for both mechanical properties, despite the ceramic having undergone a number of cycles of the $\alpha' \leftrightarrow \beta'$ transformation. This trend agrees with earlier work in Sm-Dy-sialons of designed α′:β′ ratios,[8] where the relationship was observed for as-sintered samples of different compositions. Therefore, it is clear that the reversible $\alpha' \leftrightarrow \beta'$ transformation can be used in place of compositional design to tailor the microstructure, and thus the mechanical properties, of the material.

The mechanical properties were also measured for the side face of the hot pressed samples, in order to determine the effect of preferred orientation resulting from hot pressing. The hardness and fracture toughness of the samples were determined for the side face by taking measurements at 0° and 90° to the hot pressing direction, as illustrated in Fig. 18. Thus,

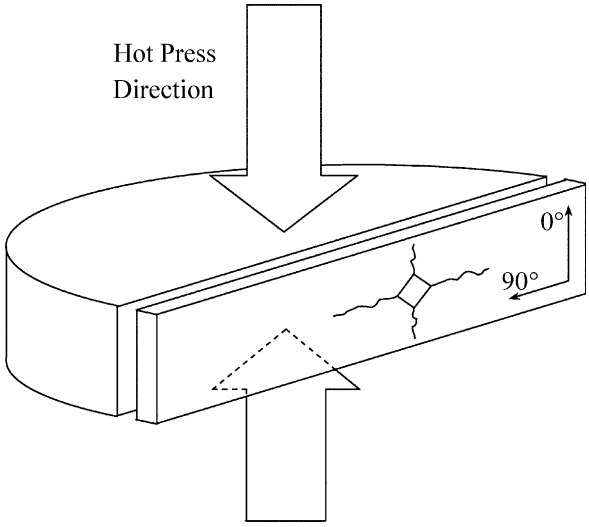

Fig. 18. Reference orientations for analysis of side faces.

2*a* and 2*c* measurements in the vertical direction were used to determine the hardness and toughness along the hot pressing direction, while horizontal measurements were used to calculate the mechanical properties normal to the hot pressing direction. These results are given in Fig. 19.

Again the cycling behaviour is evident in both the hardness and toughness of the samples, as a result of the $\alpha' \leftrightarrow \beta'$ transformation cycling. Fig. 19(a) indicates that the hardness is not greatly affected by the preferred orientation, with hard-

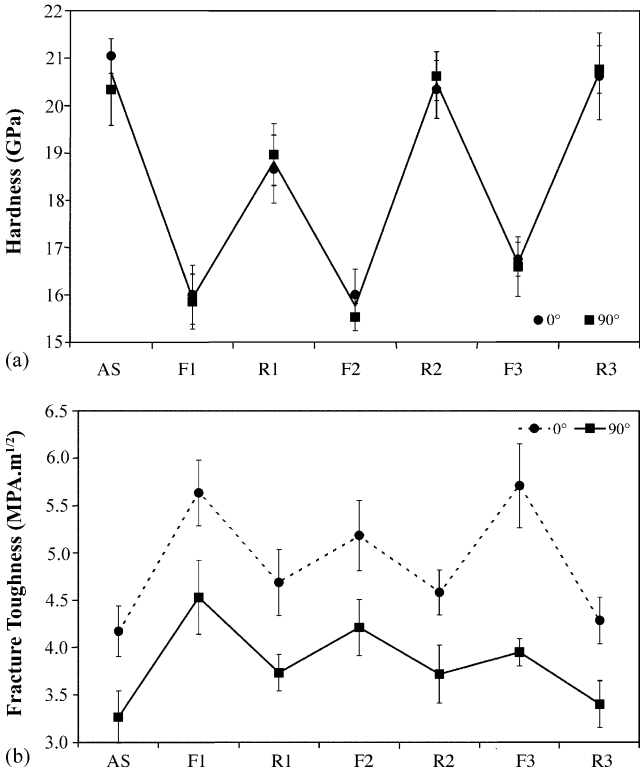

Fig. 19. (a) Vickers hardness and (b) fracture toughness of side faces of samples during transformation cycling.

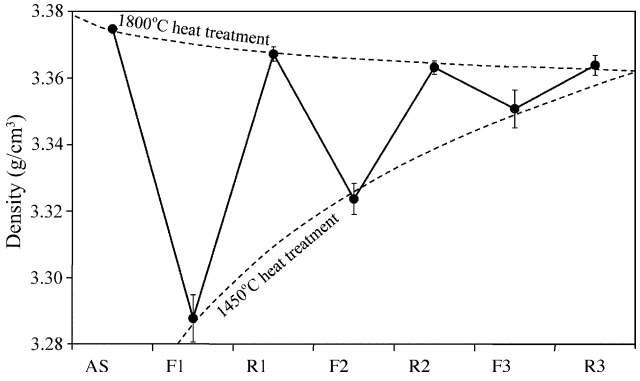

Fig. 20. Density variations during transformation cycling.

ness values easily within error for all transformation cycling stages. The toughness in Fig. 19(b), on the other hand, shows a definite difference in the orthogonal directions. The preferential orientation of α′ and β′ grains in the plane perpendicular to the hot pressing direction results in more crack deflection and grain pull-out at 0° to the hot pressing direction, while the crack is affected less at 90° to the hot pressing direction. Therefore, an increased toughness is observed. The values for the toughness at 90° to the hot pressing direction appear lower than those for the top surface in Fig. 16, however, they are largely within error. Preferred orientation has already been observed in a Ca-α-sialon, however, no mechanical properties were studied.[10] The effect of preferred orientation on the mechanical properties has been studied in hot pressed β-Si_3N_4, which showed similar variations of toughness in different orientations to the hot pressing direction.[23]

The effect of the $\alpha' \leftrightarrow \beta'$ transformation cycling on the density was investigated and is shown in Fig. 20. Again a distinct cyclic behaviour is evident, correlating with the alternating forward and reverse sialon transformation routes. The as-sintered density of 3.375 g/cm^3 indicates that hot pressing at 1800 °C for 2 h produced an essentially fully dense material. After heat treatment at 1450 °C, the density is significantly decreased. With a subsequent heat treatment at 1800 °C to promote the reverse $\beta' \rightarrow \alpha'$ transformation, the density increases, approaching the as-sintered density. Continued transformation cycling continues this trend, although the magnitude of the density changes is reduced. The decrease in density as a result of heat treatment at 1450 °C is most likely due to devitrification of the grain boundary glass. The forward $\alpha' \rightarrow \beta'$ transformation is accompanied by formation of Nd-melilite (M'_{ss}), which agglomerates into coarse pockets. This agglomeration of the grain boundary glass to form M'_{ss} is accompanied by a reduction in volume associated with changing from an amorphous, glassy state to an ordered, crystalline state. In addition, the relatively high viscosity of the Nd-rich glass at 1450 °C limits the particle re-arrangement. Therefore, the result is porosity in the bulk of the sample, as shown in Fig. 20.

Fig. 21 shows low magnification SEM micrographs of the first transformation cycle, with the pores indicated in black.

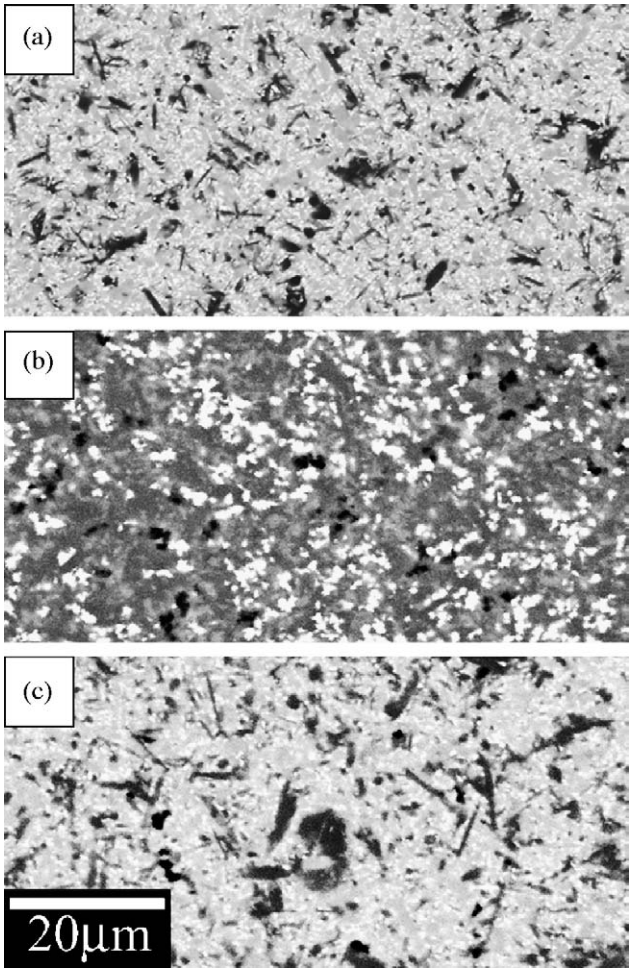

Fig. 21. SEM micrograph of bulk porosity (black) in samples (a) AS, (b) F1 and (c) R1.

The as-sintered ceramic in Fig. 21(a) clearly has no bulk porosity, confirming the full densification of the material. Heat treatment at 1450 °C has led to porosity in the sample, shown in Fig. 21(b), as a result of the $\alpha' \rightarrow \beta'$ transformation. Image analysis of the bulk porosity determined its volume fraction, as summarised in Fig. 22. It can be seen that the bulk porosity increases as α′ transforms to β′ and the grain

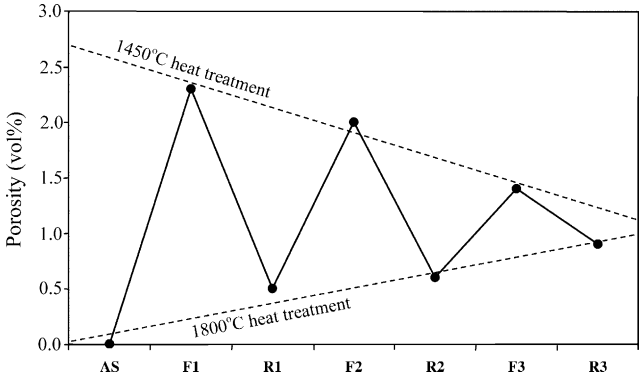

Fig. 22. Bulk porosity of samples during transformation cycling.

boundary glass agglomerates to form M'_{ss}. If the as-sintered sample is considered 100% dense, sample F1 is 97.4% dense. The bulk porosity was found to be 2.3 vol.%, which accounts for a majority of the decrease in density. The majority of the remainder is most likely due to the lower density of β′ (3.145 g/cm^3) compared to α′ (3.313 g/cm^3).[24]

Upon heat treatment at 1800 °C, the bulk porosity decreases, as shown in Fig. 21(c). The β′ → α′ transformation associated with heat treatment at 1800 °C is accompanied by melting of the secondary phase M'_{ss}, and the liquid phase redistributes and re-wets the grain boundaries. This penetration of the liquid into the microstructure fills the pores and the much lower viscosity at 1800 °C allows better particle re-arrangement to optimise packing. Therefore, a lower bulk porosity is seen in Fig. 22 and the density is increased in Fig. 20. This behaviour differs to an earlier study which found that the density decreased with heat treatment at 1450 °C for 96 h, but decreased further with additional heat treatment at 1800 °C for 1 h.[2] It is unclear why the density decreased in the earlier study when heat treated at 1800 °C, while it increased in the current work, as the SEM images in Reference 2 seem to indicate a decrease in the bulk porosity. It may have been due to surface effects, such as weight loss or oxidation, which were avoided in the current work by fully removing the surface by abrasive grinding on a diamond-embedded wheel before the density was measured.

Figs. 20 and 22 both show decreasing magnitudes in the property changes with successive heat treatments, appearing to approach equilibrium. The devitrification of the grain boundary glass and agglomeration of the secondary phase during the first α′ → β′ transformation requires a significant degree of particle rearrangement in the F1 sample. Therefore, the porosity increases. The redistribution of the grain boundary glass and particle rearrangement in sample R1 is unlikely to remove all porosity under pressureless conditions. Hence, a small residual porosity remains in the material. This residual porosity can help accommodate the agglomeration of the M'_{ss} during subsequent heat treatment at 1450 °C, reducing the need for particle rearrangement. Therefore, the porosity does not increase as much as during the first α′ → β′ transformation, and the density does not decrease as greatly. Again, the porosity cannot be removed entirely during the second heat treatment at 1800 °C, and the grain growth hinders particle rearrangement to leave a greater residual porosity in sample R2 than in R1. This larger degree of porosity will further reduce the particle rearrangement during the final α′ → β′ transformation, and the porosity and density will change less than for the previous α′ → β′ stage. Further, grain growth will restrict particle rearrangement during the final β′ → α′ transformation, leaving a, yet, greater residual porosity in the ceramic.

In addition, the α′ and β′ contents change over successive transformation cycles, as discussed in relation to Fig. 10. The remaining α′ volume fraction increases after successive forward α′ → β′ transformation stages at 1450 °C, such that the density will be higher due to the greater density of α′ than that of β′. Similarly, the α′ content is lower upon successive reverse β′ → α′ transformations at 1800 °C, so that the density will decrease between consecutive heat treatments at 1800 °C, as seen in Fig. 20.

Therefore, it can be seen from this work that the physical and mechanical properties of Nd-sialon ceramics can be tailored by appropriate heat treatment, rather than compositional design. In addition, any changes in the properties of the material that occur as a result of transformation can be countered by the appropriate heat treatment. Thus, any loss in hardness and density that results from the forward α′ → β′ transformation during use of the material at elevated temperatures may be recovered by heat treatment at 1800 °C to promote the reverse β′ → α′ transformation.

4. Conclusions

(1) A preferred orientation was observed in a Nd-sialon ceramic after hot pressing. The preferred orientation was such that the *c*-axes of the α′ and β′ phases lay preferentially in the top surface of the pellet, that is, the plane perpendicular to the hot pressing direction.

(2) Post-sintering heat treatment at 1450 °C promoted the forward α′ → β′ transformation, as evidenced by a dramatic increase in β′, accompanied by an increase in the M'_{ss} and 21R contents. This confirmed the full transformation reaction as being:

$$\alpha' + \text{liquid} \rightarrow \beta' + M'_{ss} + 21R$$

(3) Subsequent heat treatment at 1800 °C resulted in the reverse β′ → α′ transformation, which was seen as a significant decrease in the α′ content, accompanied by melting of the secondary phase M'_{ss} and the re-wetting of the grain boundary to form a uniformly distributed glass. The 21R content was also reduced during the reverse transformation, indicating that the above transformation reaction should, indeed, be:

$$\alpha' + \text{liquid} \leftrightarrow \beta' + M'_{ss} + 21R$$

(4) The preferred orientation was found to be preserved at all times, during both forward and reverse transformation routes, implying that there is a crystallographic relationship between the transformation phases during both forward and reverse routes of the α′ ↔ β′ transformation.

(5) Therefore, the α′ ↔ β′ transformation described in Eq. (6) is fully thermodynamically reversible. The microstructure is also reversible, however, there is certain degree of grain growth during reverse transformation at elevated temperatures. In addition, the composition does change over time, as evidenced by an increasing trend in the lattice parameters.

(6) The mechanical properties are affected by the α′ and β′ contents in a distinct and reproducible manner. Heat treatment at 1450 °C results in the α′ → β′ transforma-

tion, which leads to a decrease in the hardness and an increase in the fracture toughness of the ceramic. The reverse transformation at 1800 °C results in an increase in hardness and a decrease in toughness.

(7) The preferred orientation introduced by hot press sintering resulted in an anisotropic toughness, where the material had a greater fracture toughness along the hot pressing direction, due to the increased crack deflection.

(8) The density was also found to be affected by the $\alpha' \leftrightarrow \beta'$ transformation cycling, in that the density decreased with forward $\alpha' \rightarrow \beta'$ transformation and increased with subsequent reverse $\beta' \rightarrow \alpha'$ transformation. It was determined that a major contribution to the density change was due to the behaviour of the grain boundary phase.

References

1. Mandal, H., Thomson, D. P. and Ekström, T., Reversible $\alpha \leftrightarrow \beta$ sialon transformation in heat-treated sialon ceramics. *J. Eur. Ceram. Soc.*, 1993, **12**, 412.
2. Liu, Q., Gao, L., Yan, D. S. and Thompson, D. P., Thermal stability and mechanical performance of multiply heat-treated α-sialon ceramics densified with rare earth oxides. *J. Mater. Sci.*, 2000, **35**, 2229.
3. Falk, L. K. L., Shen, Z. J. and Ekström, T., Microstructural stability of duplex α-β-sialon ceramics. *Ceram. Int.*, 1997, **17**, 1099.
4. Rosenflanz, A. and Chen, I.-W., Kinetics of phase transformations in SiAlON ceramics. I. Effects of cation size, composition and temperature. *J. Eur. Ceram. Soc.*, 1999, **19**, 2325.
5. Mandal, H., New developments in α-SiAlON ceramics. *J. Eur. Ceram. Soc.*, 1999, **19**, 2349.
6. Izhevskiy, V. A., Genova, L. A., Bressiani, J. C. and Aldinger, F., Progress in SiAlON ceramics. *J. Eur. Ceram. Soc.*, 2000, **20**, 2275.
7. Zhang, C., Sun, W. S. and Yan, D. S., Characteristic of (Dy+Sm)-sialon ceramics. *Key Eng. Mater.*, 1999, **161–163**, 239.
8. Zhang, C., Sun, W. S. and Yan, D. S., Optimizing mechanical properties and thermal stability of Ln-alpha-beta-sialon by using duplex Ln elements (Dy and Sm). *J. Eur. Ceram. Soc.*, 1999, **19**, 33.
9. Mitomo, M. and Ishida, A., Stability of α-sialons in low temperature annealing. *J. Eur. Ceram. Soc.*, 1999, **19**, 7.
10. Wang, H., Cheng, Y.-B., Muddle, B. C., Gao, L. and Yen, T. S., Preferred orientation in hot-pressed Ca α-SiAlON ceramics. *J. Mater. Sci. Lett.*, 1996, **15**, 1447.
11. Gazzara, C. P. and Messier, D. R., Determination of phase content of Si_3N_4 by X-ray diffraction analysis. *Ceram. Bull.*, 1977, **56**, 777.
12. Shen, Z. and Nygren, M., On the extension of the α-sialon phase area in yttium and rare-earth doped systems. *J. Eur. Ceram. Soc.*, 1997, **17**, 1639.
13. Hewett, C. L., Cheng, Y.-B., Muddle, B. C. and Trigg, M. B., Thermal stability of calcium α-sialon ceramics. *J. Eur. Ceram. Soc.*, 1998, **18**, 417.
14. Anstis, G. R., Chantikul, P., Lawn, B. R. and Marshall, D. B., A critical evaluation of indentation techniques for measuring fracture toughness. I. Direct crack measurements. *J. Am. Ceram. Soc.*, 1981, **64**, 533.
15. Cheng, Y.-B. and Thompson, D. P., Aluminum-containing nitrogen melilite phases. *J. Am. Ceram. Soc.*, 1994, **77**, 143.
16. Zhao, H., Swenser, S. P. and Cheng, Y.-B., Elongated α-sialon grains in pressureless sintered sialon ceramics. *J. Eur. Ceram. Soc.*, 1997, **18**, 1053.
17. Hwang, S.-L. and Chen, I.-W., Nucleation and growth of β′-SiAlON. *J. Am. Ceram. Soc.*, 1994, **77**, 1719.
18. Zhao, R., Swenser, S. P. and Cheng, Y.-B., Formation of AlN-polytypoid phases during α-SiAlON decomposition. *J. Am. Ceram. Soc.*, 1997, **80**, 2459.
19. Zhao, R. and Cheng, Y.-B., Decomposition of Sm α-SiAlON phases during post-sintering heat treatment. *J. Eur. Ceram. Soc.*, 1996, **16**, 1001.
20. Shen, Z., Ekström, T. and Nygren, M., Homogeneity region and thermal stability of neodymium-doped α-sialon ceramics. *J. Am. Ceram. Soc.*, 1996, **79**, 721.
21. Hwang, S.-L. and Chen, I.-W., Nucleation and growth of α-SiAlON on α-Si_3N_4. *J. Am. Ceram. Soc.*, 1994, **77**, 1711.
22. Cheng, Y.-B. and Thompson, D. P., Pressureless sintering and phase relationship of samarium α-sialons. *J. Eur. Ceram. Soc.*, 1994, **14**, 343.
23. Lee, F. and Bowman, K. J., Texture and anisotropy in silicon nitride. *J. Am. Ceram. Soc.*, 1992, **75**, 1748.
24. Powder diffraction files from JCPDS-ICDD “PCPDFWIN” software program.